Korean J. Chem. Eng., 38(11), 2256-2264 (2021)
DOI: 10.1007/s11814-021-0872-7

pISSN: 0256-1115
eISSN: 1975-7220

Novel application of the esterification product of 2,3-dihydroxybutanedioic acid and cellulosic biomass for cobalt ion adsorption

Ali Hashem*,†, Chukwunonso Onyeka Aniagor,†, Sayed Mohamed Badawy***, and Ghada Mohamed Taha***

*Textile Research Division, National Research Centre, Dokki, Cairo, Egypt
**Department of Chemical Engineering, Nnamdi Azikiwe University, P.M.B. 5025, Awka, Nigeria
***National Center for Clinical and Environmental Toxicology, Faculty of Medicine, Cairo University, Egypt
(*Received 25 March 2021 • Revised 12 June 2021 • Accepted 19 June 2021*)

Abstract−A novel biosorbent (*'Manna_COOH'*) was synthesized via dual reaction stages of direct carbonylation of hydroxyl groups of richly cellulosic manna root powder and subsequent esterification of the resultant anhydride analogue into an ester of high carboxyl content. Both the biosorbent precursor and the 2,3-dihydroxybutanedioic acid sustain complementary features that ensured their efficient complexation. The biosorbent depicted a carboxyl content of 412.36 m.eq -COOH/100 g sample and was characterized using scanning electron microscopy (SEM), X-ray diffraction (XRD), and Fourier-transform infrared spectroscopy (FTIR). The study further evaluated the cobalt ion adsorption capacity of the synthesized *'Manna_COOH'* under the effect of some process variable via batch mode. The Freundlich and pseudo-second-order models emerged as the best fit for the equilibrium and kinetic data, respectively. The rich oxygen-based surface functional groups entrenched on the *'Manna_COOH'* sequel to its functionalization played a major role in making it a promising biosorbent for aqueous Co (II) uptake.

Keywords: Adsorption, Cobalt Ion, Biosorbent, Isotherm, Kinetics

INTRODUCTION

The issue of heavy metal pollution is a major threat to environmental sustainability, human health and mankind development [1]. Cobalt is a typical heavy metal that is extensively utilized in several process industries, especially during paint and lithium-ion battery production [2,3]. Thus, the aforementioned processes account for the majority of cobalt ion contamination in the aqueous environment due to poor effluent discharge habits of the respective industries [4] and lenient waste disposal regulations. While cobalt occurs naturally and is also considered a micronutrient, human exposure to its high concentration could be carcinogenic, as well as portend other health issues (such as dermatitis, mild paralysis, etc.) [5-7].

In this regard, the development of an efficient treatment system to proffer a long term solution to recurrent heavy metal pollution is greatly desired. Consequent upon decades of research, several treatment techniques which include adsorption [8-12], ion exchange [13,14], membrane filtration [15-17], etc. have been successfully investigated. Considering the respective characteristics, merits, demerits and applicabilities of each technique, adsorption is seen as a worthwhile option on account of its low operational cost and versatility, as well as its high treatment efficiency [18-21]. Its application of agro-based/eco-friendly adsorbents, which makes for an absolute greened water-treatment option, is another important advantage of the adsorption technique [22,23].

Numerous studies have evaluated the heavy metal sorption capacity of different agro-based materials, including natural polymers [24-28]. Notably, these polymers (such as starch, cellulose, and chitosan) are environmentally friendly, renewable and relatively economical [1]. Despite the aforementioned benefits, the sorption properties of the untreated version of these polymers are usually unacceptable, hence the need for their functionalization. Also, studies [1,29,30] have shown that hydroxyl and carbonyl groups, which are the major constituents of natural polymers, are usually not potent for cation binding. Consequently, the introduction of carboxyl functional groups (via chemical functionalization) is often adopted to effectively compensate for their poor metal ion sorption performance. Balaska et al. [31], and Hashem et al. [32] observed some improvement in the metal sorption capacity of juniper fibre and sawdust, respectively upon their chemical functionalization. According to the studies, the chemical functionalization afforded the carboxyl group which subsequently supplied the important sites required for the metal ion binding through the formation of carboxylate salts.

In this study, a novel biosorbent (*'Manna_COOH'*) was obtained through dual reaction stages of direct carbonylation of hydroxyl groups, -OH (using 2,3-dihydroxybutanedioic acid) and subsequent esterification of the resultant anhydride analogue into ester of high carboxyl (-COOH) content. The richly cellulosic massive root structure of the unpalatable, cheaply available and invasive manna trees, was used as the biosorbent precursor. The invasive nature of this tropical plant makes their elimination from an invaded farmland very challenging [33]. Hence, the aforementioned reasons (its invasiveness, cheap availability and rich cellulosic content) justify the choice of the manna tree as a biosorbent precursor in this study. Furthermore, both the biosorbent precursor (the polymeric manna

†To whom correspondence should be addressed.
E-mail: alihashem2000@yahoo.com, co.aniagor@unizik.edu.ng

tree root powder) and the 2,3-dihydroxybutanedioic acid sustain complementary features. For instance, the polymer is cheaply available, but with poor metal ion sorption capacity which is linked to the absence of the relevant carboxyl groups. Conversely, the organic acid which subsequently reacted with the polymer -OH groups to afford the desired esters of abundant -COOH groups is a liquid, hence cannot be applied as a sole adsorbent. The study further evaluated the cobalt ion adsorption capacity of the synthesized *'Manna_COOH'* under the effect of certain process variable via batch mode. The physicochemical, morphological and structural characteristics, as well as the equilibrium and kinetic modelling behavior of the *'Manna_COOH',* was also elucidated in the study.

MATERIALS AND METHODS

1. Materials

The manna tree was collected from the Matrouh desert, Egypt. The reagents used in the study, which include cobalt acetate, 2,3-dihydroxybutanedioic acid, ethanoic acid, sodium carbonate, acetone, and ethyl alcohol, were all laboratory grade chemicals, supplied by Merck, Germany.

2. Preparation of the Adsorbent

The root of the manna tree was carefully harnessed, washed with distilled water, oven-dried at 80 °C for 10 h and then ground to fine particle sizes in the range of 50-125 μm. Afterwards, 2.0 g of the powdered root material was digested in 80 wt% 2,3-dihydroxybutanedioic acid, whose volume is sufficient enough to achieve a slurry, contained in a flask followed by manual stirring until complete homogenization. The obtained slurry was then oven-dried at 100-150 °C and subsequently cooled to room temperature. To eliminate any unreacted acid and by-products, the desired dried sample was washed with 80 wt% ethanol and finally oven-dried at 80 °C until constant dry weight to yield the *'Manna_COOH'* adsorbent.

3. Measurement of the Carboxyl Content of *'Manna_COOH'*

50 mL of 0.03 N NaOH solution was charged into a conical flask containing a given amount of *'Manna_COOH' (about* 0.2 g) and the mixture was left to stand overnight at 25 °C. After equilibration, the mixture was titrated with 0.01 N HCl solution using a phenolphthalein indicator. Meanwhile, a duplicate experiment was performed in the absence of the *'Manna_COOH'* adsorbent Thus, by applying Eq. (1) [34], the carboxyl content was further evaluated.

$$[\text{COOH}]\text{m. eq/100 g. sample} = \frac{(V_0 - V_1)N}{W} \times 100 \quad (1)$$

where V_1 and V_o are the HCl volume (mL) consumed in the presence of *'Manna_COOH'* adsorbent and blank experiment, respectively, N is the normality of the HCl solution, and W=amount of the *'Manna_COOH'* used (g).

4. Adsorption Experiments

By dissolving an appropriate amount of cobalt acetate in deionized water, a stock solution of the adsorbate (1 g L^{-1}) was obtained. Meanwhile, the working cobalt ion concentrations were further achieved from the serial dilution (using deionized water) of the stock solution.

During the adsorption experiment, a predetermined amount of *'Manna_COOH'* was charged into the adsorbate solution (100 mL) contained in a 250 mL conical flask. The mixture was stirred mechanically on a magnetic stirrer (Stuart, Model UC151/120 V/60) at 150 rpm and 30 °C. At a specified interval, test samples were withdrawn from the mixture, filtered through Whatman No. 41 filter paper and the remaining cobalt ion concentration was measured using atomic absorption spectrophotometer (AAS, ZA3000, HITACHI, Japan). By varying the solution pH using either 0.1 M HNO_3 or 0.1 M NaOH as appropriate, the effect of pH studies was investigated in the pH range of 2.0-7.0. Similarly, the effect of time (0-180 min) and adsorbent dosage (0.03 to 0.8 g/L) was also investigated.

The associated adsorption parameters such as the % removal efficiency (RE %), as well as the amount of cobalt ion adsorbed at equilibrium (q_e), are calculated from Eqs. (2) and (3), respectively.

$$\text{RE}\ (\%) = \frac{C_o - C_e}{C_o} \cdot 100\% \quad (2)$$

$$q_e = \frac{(C_o - C_e)V}{W} \quad (3)$$

where C_o=Initial cobalt ion concentration (mg L^{-1}), C_e=cobalt ion concentration at equilibrium (mg L^{-1}), W=Mass of *'Manna_COOH'* used (g), V=volume of adsorbate solution used (L).

RESULTS AND DISCUSSION

1. The Various Characteristic Process Mechanisms

1-1. Adsorbent Synthesis Mechanism

The different reactions relating to the synthesis of the *'Manna_COOH'* are explained in this section. Upon the impregnation of the adsorbent precursor (manna root powder) in the 2,3-dihydroxybutanedioic acid and their subsequent oven-drying, two major reactions occur: (a) the heat catalyzed conversion of the carboxylic group of the 2,3-dihydroxybutanedioic acid to its anhydride analog [Eq. (4)], (b) the consequent esterification of the formed anhydride groups with the hydroxyl groups of the cellulosic manna root powder to yield the desired ester of high carboxyl content of 412.36 m.eq -COOH/100 g sample [Eq. (5)].

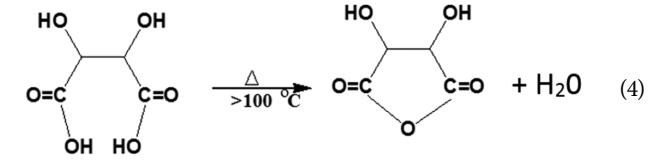

(4)

[2,3-dihydroxybutanedioic acid] [2,3-dihydroxybutanedioic anhydride]

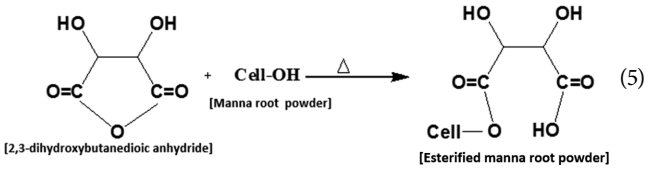

(5)

[2,3-dihydroxybutanedioic anhydride] [Esterified manna root powder]

1-2. Adsorption Mechanism

The oxygen-based (-OH and C-O) functional groups introduced during the carboxylic acid functionalization of the adsorbent, as elucidated later in the FTIR analyses section, provided abundant binding sites for cobalt ion sequestration. By exploiting these sorption sites on these oxygen-based functional groups, coupled with

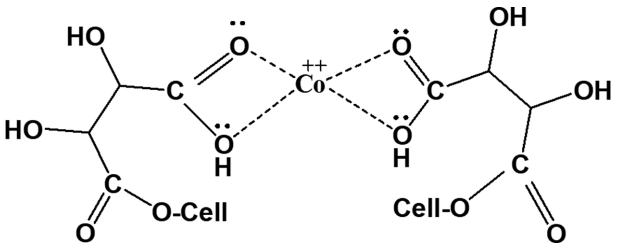

Scheme 1. The schematic representation of the probable adsorption mechanism.

the large coordination number of Co (II) ion, an electrostatic interaction mechanism is forged as shown in Scheme 1. Furthermore, Scheme 1 schematically illustrates that each of the O-atoms offered an electron lone pair for cobalt ion binding. Thus, electrostatic interaction/complexation between the oxygen-containing functional groups and the Co (II) ion is considered as the probable adsorption mechanism involved in the study.

2. FTIR Analyses

FTIR spectra for samples were obtained via the KBr disk technique using test scan FT-IR spectrometer 4100 JASCO - JAPAN. The spectra were recorded in the range of 400-4,000 cm^{-1} (scanning speed: 2 mm/sec, resolution: 4 cm^{-1}) and the obtained diffractogram for the adsorbent precursor (manna root powder), *'Manna_COOH'* and Co (II)-loaded *'Manna_COOH'* are shown in Figs. 1(a)-(c).

The observed spectra difference between the trace-line 'a' (adsorbent precursor) and trace-line 'b' (organic acid modified adsorbent, *'Manna_COOH'*) is evidence for the occurrence of successful esterification reaction The precursor sample, exhibited a broad absorption peak at 3,427 cm^{-1} assigned to the bonded and free O-H vibrations groups of cellulose and adsorbed water. The peak at 2,920 cm^{-1} is due to the stretching vibration of the C-H bond of methyl groups, while the strong peaks at 1,629 cm^{-1} are characteristic of carbonyl group stretching in the sample. The strong stretching vibration of C-O (1,051 cm^{-1}) is specific to the lignin and hemicellulosic components [35]. The organic acid modified *'Manna_COOH'* (Trace b), shows the appearance of a new peak at 1,751

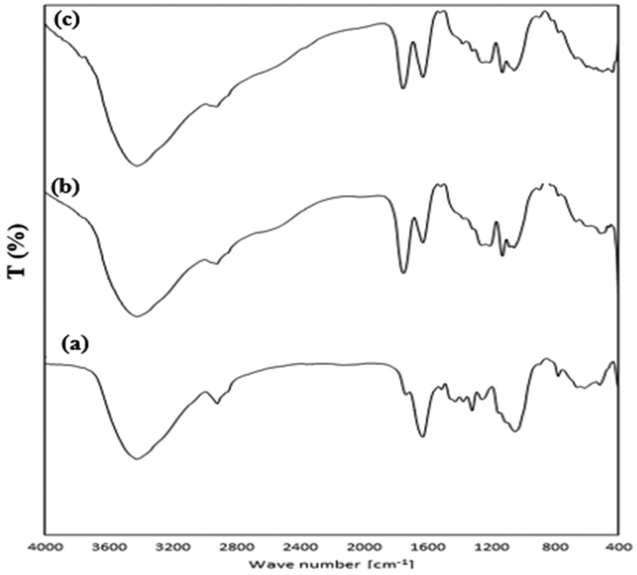

Fig. 1. FTIR spectra for (a) Manna root powder (b) 'Manna_COOH' and (c) Co (II)-loaded 'Manna_COOH'.

cm^{-1} due to the absorption of carbonyl stretching of carboxylic acid ester groups after thermal treatment with 2,3-dihydroxybutanedioic acid [10]. The peak at 1,130 cm^{-1} is attributed to the C-O stretching vibration of carboxyl groups. Trace line 'c' of Fig. 1 shows a broadening of the O-H vibration peak, attributed to complexation with the Co(II) ions and vibrations of O-H groups from water molecules coordinated to the metal ions [36].

3. SEM Analyses

The surface morphology of the adsorbent precursor (manna root powder), synthesized adsorbent (*'Manna_COOH'*) and spent adsorbent (Co(II)-loaded *'Manna_COOH'*) was obtained using SEM measurement [TESCAN CE VEGA 3 SBU (117-0195- Czech Republic)] at 1,000x magnification. Meanwhile, the corresponding SEM micrographs are presented in Figs. 2(a)-(c). The micrograph of the adsorbent precursor as depicted in Fig. 2(a) is characterized by a rumpled paper-like overlapping structure. Minimal surface roughness and porosity were also evidenced (Fig. 2(a)). A more elabo-

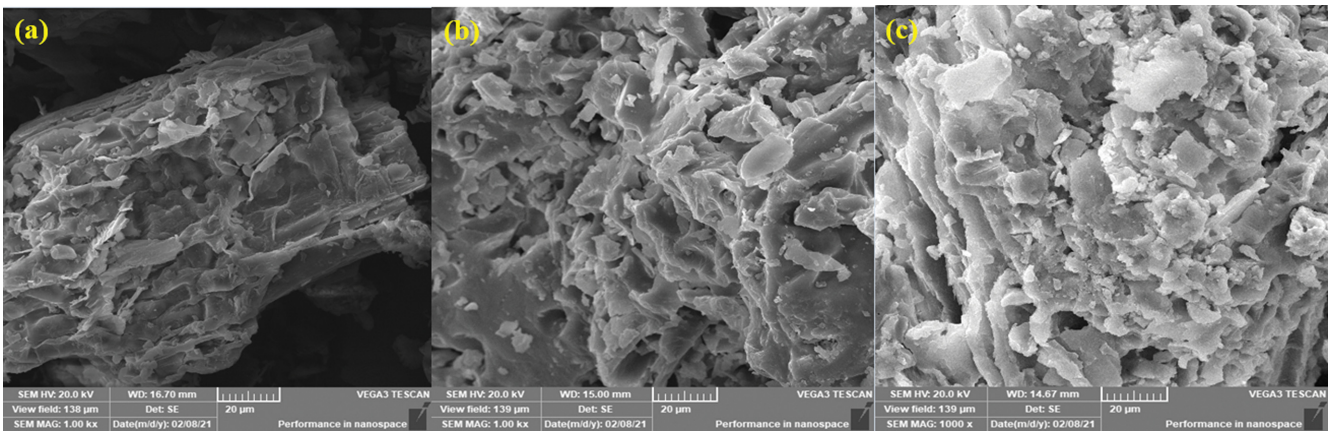

Fig. 2. SEM images for (a) Manna root powder (b) 'Manna_COOH' and (c) Co (II)-loaded 'Manna_COOH'.

rate porous structure and surface roughness which is synonymous with enhanced metal ion chelation was observed in Fig. 2(b), following the esterification reaction. A comparative investigation of Fig. 2(b) (unloaded *'Manna_COOH')* and Fig. 2(c) (Co(II)-loaded *'Manna_COOH')* showed negligible surface structural differences. However, the SEM micrograph of the metal loaded adsorbent became brighter, probably due to the presence of the adsorbed cobalt ion.

4. X-ray Analyses

X-ray diffraction (XRD) analysis was performed via a continuous scanning mode on a diffractometer of PANalytical diffractometer (X'Pert PRO) and the diffraction intensity was recorded from 2° to 60°. The obtained diffractograms for the adsorbent precursor (manna root powder), *'Manna_COOH'* and Co (II)-loaded *'Manna_COOH'* are shown in Fig. 3(a)-(c). The respective XRD patterns show features typical of a cellulosic material $(C_6H_{10}O_5)_n$, with certain sharp and broads diffraction peaks indicative of the crystallinity and amorphous background undertone, respectively. Fig. 3(a) shows the major peaks at 2θ=15.07°, 24.45° and 38.27°. Though the crystallinity index data were not provided, the sharp diffraction peaks are an indication of the presence of the highly crystalline cellulose phase (cellulose I β) [37] (JCPDS card no00-056-1718). The broadening of a peak at 2θ=22.81° is due to the presence of the amorphous cellulose phase. Meanwhile, the post-modification XRD spectrum of *'Manna_COOH'* (Fig. 3(b)) shows no significant variation from that of the adsorbent precursor (manna root powder), thus indicating that the crystallinity and fibrous structure of the cellulosic material was neither altered nor damaged sequel to their chemical interaction with 2,3-dihydroxybutanedioic acid. This finding that the esterification reaction probably occurred in the amorphous structure of cellulosic material [32]. The post-adsorption XRD spectrum (Fig. 2(c)) indicates that the complexation of the cobalt ion with the adsorbent during adsorption resulted in the weakening and intensity reduction in the peaks previously observed in the unloaded-*'Manna_COOH'* diffractogram. This finding suggests the non-discrete distribution of relatively disordered phase all through the Co(II)-loaded *'Manna_COOH'* structure.

5. Effect of Process Variables

5-1. Effect of pH

The electrostatic charges on the *'Manna_COOH'* surface functional groups could be significantly altered when the adsorbent is subjected to changes in pH [38]. Meanwhile, this surface charge alteration also has a strong effect on the *'Manna_COOH'* cation sorption capacity. Fig. 4(a) graphically illustrates the effect of variation in solution pH on the cobalt ion adsorption capacity of *'Manna_COOH'* at a constant time (120 min), initial cobalt ion concentration (300 mg/L) and adsorbent dosage (0.03 g/L). However, a consistent improvement in the adsorption capacity was witnessed upon the increase in the solution pH up to pH 6.0. Meanwhile, a further solution pH increase beyond pH 6.0 resulted in a decreased adsorption capacity. This finding is as expected since the adsorbents' pH_{PZC} was recorded at pH 4.1 (plot not shown), hence the *'Manna_COOH'* surface charge is protonated and deprotonated, respectively, at low ($pH<pH_{PZC}$) and high ($pH>pH_{PZC}$) solution pH. However, the implication is that at increased surface charge protonation the metal cation is electrostatic repelled, hence the ob-

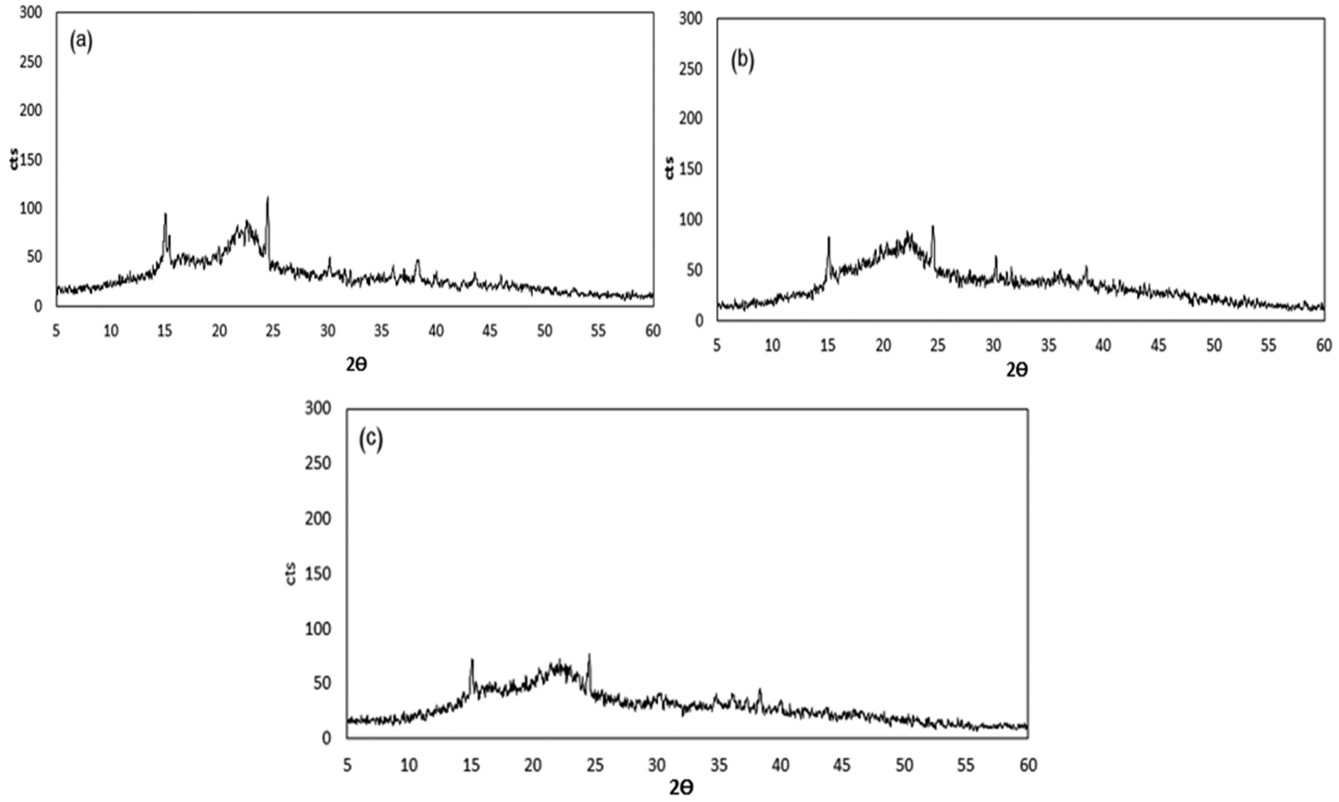

Fig. 3. XRD diffractogram for (a) Manna leaves (b) 'Manna_COOH' and (c) Co (II)-loaded 'Manna_COOH'.

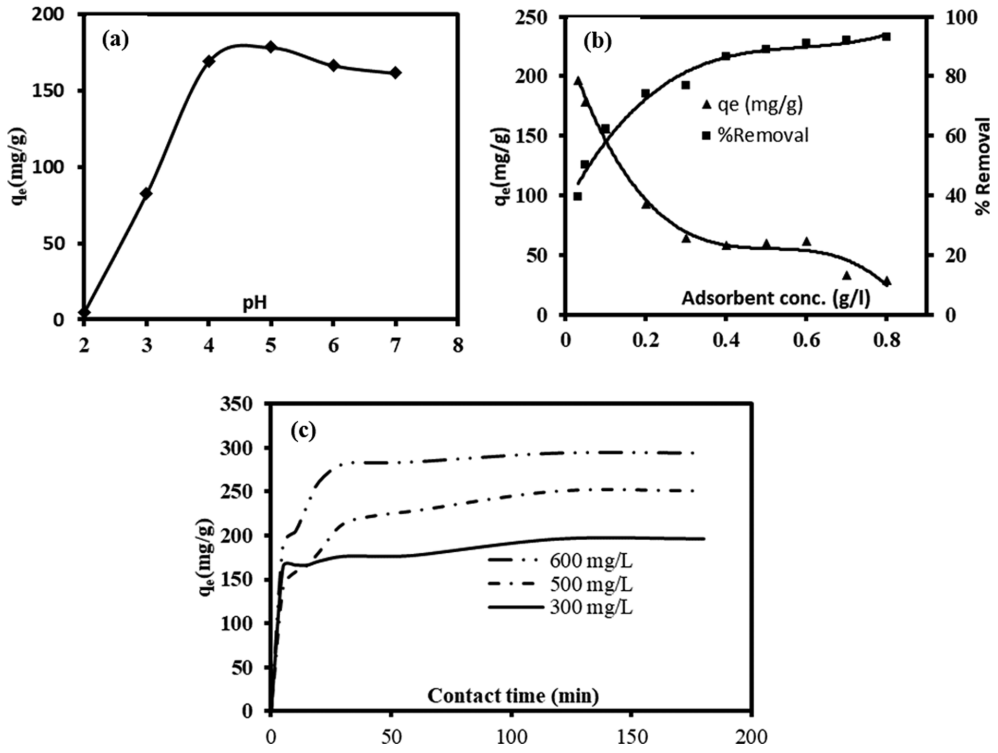

Fig. 4. The plot of the effect of (a) solution pH on the adsorbed amount, (b) adsorbent conc. on the % removal and adsorbed amount, (c) variation of contact time and initial concentration on the adsorbed amount.

served reduction in adsorption capacity and vice versa at surface charge deprotonation [39]. Consequently, preliminary studies by the authors showed that an increase in the solution pH beyond pH 6.0 and deep into the alkaline region resulted in a sustained adsorption capacity decrease due to probable precipitation of the cobalt ion as a hydroxide. Therefore, pH 6.0 was recorded as the solution pH for optimum adsorption of cobalt ion.

5-2. Effect of Adsorbent Dosage

The effect of the adsorbent concentration (g/L) on the *'Manna_COOH'* adsorption capacity (mg/g) and removal efficiency (%) was simultaneously investigated, with the corresponding plot presented in Fig. 4(b). This investigation was conducted at a constant time (120 min), initial cobalt ion concentration (300 mg/L) and solution pH (pH 6.0). The adsorption capacity was observed to depict an inverse variation with the removal efficiency, meanwhile, removal efficiency shows great disparity with changes in the initial concentration. Therefore, in this study, only the relationship between that adsorbent dosage and adsorption capacity will be emphasized, since the latter is a function of the intrinsic adequacy of the adsorbent [40-42].

According to Fig. 4(b), a trend of sustained decrease in the adsorption capacity with an increase in the amount of *'Manna_COOH'* at every instant was observed. It was further shown that an increase in the adsorbent mass (from 0.03 to 0.8 g/L) resulted in a sharp decline (about 85.2% reduction) in the *'Manna_COOH'* adsorption capacity. Hence, the adsorption capacity ultimately reduced from 196.77 mg/g (at 0.03 g of *'Manna_COOH'*/liter of adsorbate) to as low as 29.11 mg/g (at 0.8 g of *'Manna_COOH'*/liter of adsorbate). This observation could be linked to the possible active site clogging, overcrowding and subsequent agglomeration at high adsorbent dosage [43,44]. The decrease in the adsorption capacity with increased adsorbent dosage could also be due to the availability of more active sites of adsorbent which progressively remained unsaturated during the adsorption process [45,46].

Therefore, an optimum *'Manna_COOH'* mass of 0.03 g/L was subsequently adopted in the study.

5-3. Combined Effect of Contact Time and Initial Adsorbate Concentration

The combined effect of contact time and initial adsorbate concentration as presented in Fig. 4(c) showed three (3) kinetic stages.

The first stage existed within the initial 5 min of the batch experiment, where the respective adsorption (300, 500 and 600 mg/L) systems show a fast adsorption rate and averaging about 60% of the total adsorption capacity recorded at the optimum contact time. Critical observation of Fig. 4(c), however, showed that the sorption rate decreased with an increase in the initial adsorbate concentration. For instance, in the case of the 300 mg/L system, 165.6 mg/g (about 84%) of its optimum adsorption capacity (196.7 mg/g) was achieved in the first (5 min) adsorption stage, whereas the 500 mg/L and 600 mg/L systems, respectively achieved only about 56% and 65% of their optimum adsorption capacity. This observation is linked to a reduction in the adsorbates' chemical potential at such higher initial concentrations, thus limiting their driving force [47].

Between the time interval of 10 and 60 min, a general abatement of adsorption rate was witnessed for all adsorption systems. However, the adsorption systems of higher initial adsorbate concentra-

tions (500 and 600 mg/L) recorded an improved rate, attaining about 31% (for 600 mg/L) and 28% (for 500 mg/L) of their optimum adsorption capacity, as compared to the 6% achieved for the 300 mg/L system. This observation illustrates that the 500 and 600 mg/L systems depicted a higher driving force in comparison with the 300 mg/L system within this adsorption stage [48].

The third adsorption kinetic stage signified the equilibration of the adsorption capacity at 120 min. Thus, to ensure adsorption equilibrium a contact time of 120 min was adopted for the study.

6. Equilibrium Studies

The study was executed by modelling the experimental equilibrium data with two (2) classical isotherm models: Langmuir and Freundlich models. Due to the insufficiency of the coefficient of determination alone as a criterion for selecting the model of best fit, a nonlinear error function, average percentage error (APE) was introduced. The mathematical expression of the APE is presented in Eq. (6). However, the isotherm model that depicts the smallest APE-value is believed to provide a minimal error variance between the experimental and model-predicted adsorption capacity values, hence is regarded as the best fit [32]. The fitting of the respective isotherm moels to the equilibrium experimental data is discussed further in the subsequent subsections, while the combined isotherm plot and parameter table for both models are presented in Fig. 5 and Table 2, respectively.

$$\mathrm{APE}(\%)=\frac{\sum_{i=1}^{n}\left|(q_{e,\,exp}-q_{e,\,pred})/q_{e,\,exp}\right|}{n}*100 \tag{6}$$

where 'n' is the number of the experimental data point.

6-1. Langmuir Model

This model is hinged on the fundamental assumption of monolayer adsorption onto a homogenous adsorbent surface, with identical/energetically uniform adsorption sites. The nonlinear Langmuir model equation and the associated favorability constant (R_L) is expressed as Eq. (7)-(8) [49]. Where $R_L>1$, $R_L=1$, $R_L=0$ and $0<R_L<1$ implies unfavorable, linear, irreversible and favorable nature of the adsorption process, respectively.

$$q_e=\frac{q_m k_L C_e}{1+k_L C_e} \tag{7}$$

$$R_L=\frac{1}{1+K_L C_o} \tag{8}$$

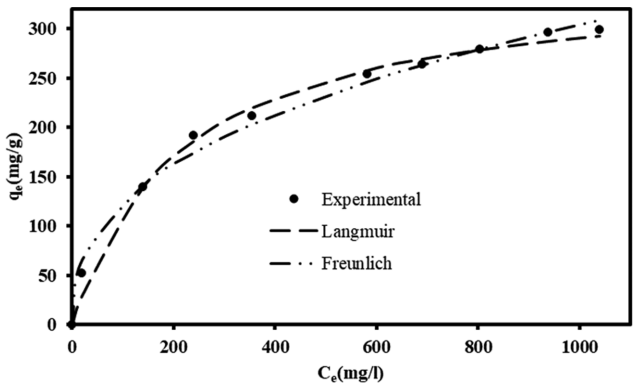

Fig. 5. The equilibrium isotherm plot.

Table 1. The isotherm model parameters

Langmuir		Freundlich	
q_{max}=353.56	K_L=1.644	n_F=2.56	K_F=20.51
R^2=0.999	APE=0.180	R^2=0.999	APE (%)=0.089
R_L=4.6E-03			

According to Table 1, this model showed a sufficiently large maximum adsorption capacity of 353.56 mg/g. Similarly, the models' separation factor, R_L, depicted a positive value of 4.6E-03 ($0<R_L<1$), thus suggesting adsorption favorability. Its coefficient of determination (R^2) and APE values of 0.999 and 0.180, respectively, is relatively good and within a suitable range. Although its R^2 value is sufficiently high, the APE value is inferior to those recorded by the Freundlich model. Therefore, the Langmuir model cannot be regarded as the best fit, although its predicted data provided a reasonable fit to the experimental data as depicted in Fig. 5.

6-2. Freundlich Model

This model is synonymous with heterogeneous multilayer adsorption and uneven adsorption energy distribution [50]. The model is mathematically expressed as Eq. (9), while the model constant (n_F) value suggests the extent of the adsorbent-adsorbate affinity.

$$q_e=K_F(C_e)^{\frac{1}{n_F}} \tag{9}$$

The fitting of the equilibrium experimental data to this model as shown in Fig. 5 depicted the highest R^2 and the lowest APE values of 0.999 and 0.089, respectively (Table 1). Based on these values, the model predicted data is believed to have provided the best description of experimental data. Similarly, the evaluated n_F value of 2.56 is well within the expected range ($1<n_F<10$), thus implying a favorable interaction between the cobalt ion and the *'Manna_COOH'* adsorbent. Consequently, the adsorbate sustained a heterogeneous multilayer binding onto the *'Manna_COOH'* surface.

7. Kinetic Studies

The pseudo-first-order and pseudo-second-order kinetic models were applied for the modelling of the experimental kinetic data. The mathematical expression of these models and further discussions on the import of their respective parameters (at different initial adsorbate concentrations) are presented in the following subsections. Meanwhile, the best fit model was decided based on the magnitude of the APE-value that is evaluated from Eq. (6).

7-1. Pseudo-first Order (PFO) Model

The plot and the parameters deduced from this model under varying initial adsorbate concentrations (300, 500 and 600 mg/L) are presented in Fig. 6 and Table 2, respectively. It was observed that the first-order rate constant (k_1) decreased with an increase in the initial adsorbate concentration. This observation could be due to a reduction in the adsorbates chemical potential at high initial concentration, thereby resulting in reduced adsorption driving force. Conversely, the modelled adsorption capacity ($q_{e\,cal}$) consistently appreciated with increment in the initial concentration, thus suggesting a decreased mass transfer resistance and the occurrence of physisorption at higher adsorbate concentrations [51,52]. Furthermore, the R^2 value was reasonably high (>0.9) at all initial concen-

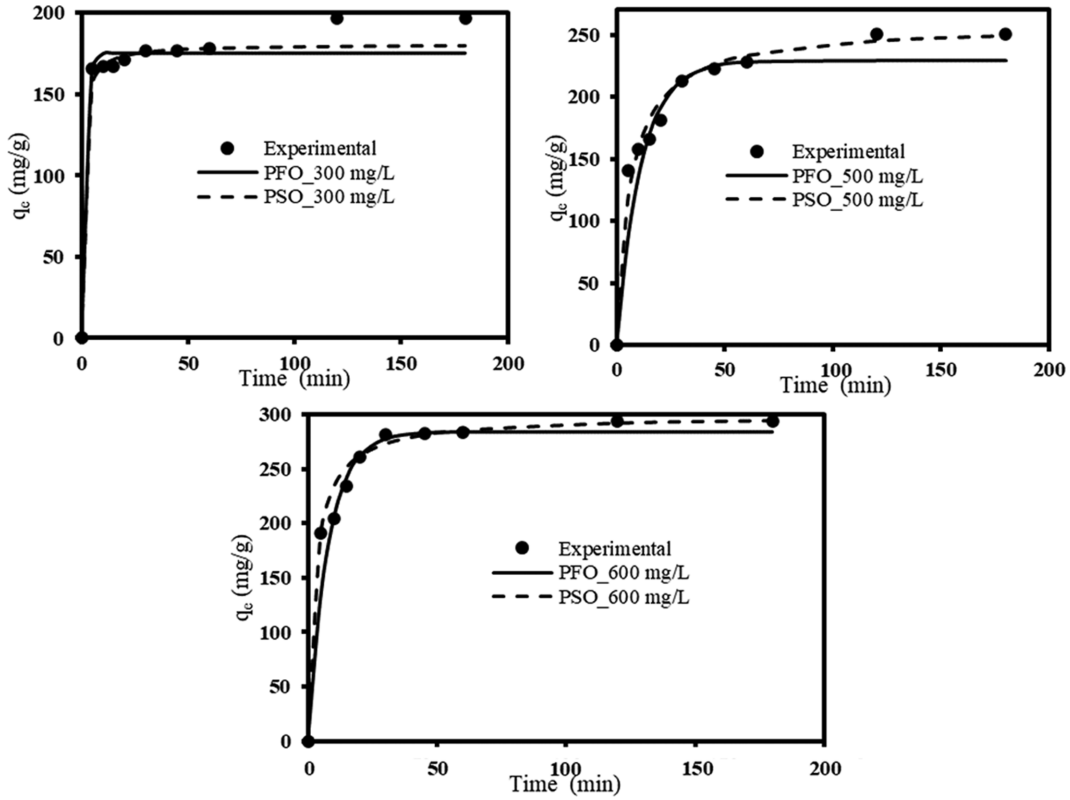

Fig. 6. Plots of the Experimental, Pseudo-first-order, and Pseudo-second-order kinetics data at varying initial concentrations.

Table 2. Kinetic model parameters

300 mg/L	500 mg/L	600 mg/L
Pseudo-first-order		
q_e=175.479	q_e=229.07	q_e=284.092
k_1=0.576	k_1=0.127	k_1=0.088
R^2=0.995	R^2=0.994	R^2=0.986
APE=0.029	APE=0.093	APE=0.214
Pseudo-second-order		
q_e=189.491	q_e=258.417	q_e=298.953
k_2=6.8E-03	k_2=1.1E-03	k_2=6.0E-04
R^2=0.997	R^2=0.998	R^2=0.997
APE=0.020	APE=0.026	APE=0.054

*qe, exp@300 mg/L=196.77 mg/g; qe, exp@500 mg/L=250.33 mg/g; qe, exp@300 mg/L=293.91 mg/g

trations, while the APE value, although small in all cases (in the range of 0.093 to 0.214), is still larger than those of the pseudo-second-order model. Similarly, the maximum adsorption capacity ($q_{e,Cal}$) determined at all the initial concentrations were higher than the experimental adsorbed amounts ($q_{e,Exp}$). This inconsistency in the $q_{e,Cal}$ and $q_{e,Exp}$, as well as the relatively large APE value, indicates the inferiority of the PFO predicted data when compared to those of the PSO.

7-2. Pseudo-second Order (PSO) Model

The data fitting pseudo-second-order (PSO) model to the experimental data was the best, as the model depicted high R^2 values (R^2>0.99) and lowest APE values (0.02-0.054) (Table 2) The PSO model curve shown in Fig. 6 had a better fit to the experimental data curve line at all studied concentrations. Also, just as in the case of the PFO model, the second-order rate constant (k_2) showed a similar decreasing trend with increased initial concentration, while the modelled adsorption capacity increased with increasing adsorbate concentration (Table 2). The improvement in the adsorption capacity with an increase in the initial adsorbate concentration is still related to the occurrence of limiting mass transfer resistance as already mentioned in the previous subsection. Additionally, the correlation between the $q_{e,Cal}$ and $q_{e,Exp}$-values further buttress the superiority of the PSO to the PFO for the experimental data modelling.

8. Comparison of the Manna_COOH Cobalt Ion Adsorption Capacity with that of other Adsorbents

Table 3 shows the comparison of cobalt ion adsorption capacity of Manna_COOH with those of previously applied cellulose-based sorbents in descending order of magnitude. The adsorption capacity recorded in this study is higher than that of other sorbents reviewed except for magnetized α-cellulose fibres. Therefore, it can be concluded that the prepared esterified manna root powder (Manna_COOH) is a promising and useful adsorbent for the removal of aqueous cobalt ions.

CONCLUSION

By adopting the richly cellulosic massive root structure of the unpalatable, readily available, invasive and irritating manna trees

Table 3. Comparison of adsorption capacities of various sorbents for cobalt ions

Adsorbent	Adsorption capacity (mg/g)	Reference
Magnetized α-cellulose fibers	1,567.0	[53]
Esterified manna root powder (Manna_COOH)	293.91	Present study
Butandioic acid modified cellulose	188.67	[54]
Citric acid-modified orange peel cellulose	75.43	[55]
Oxalic acid-modified orange peel cellulose	66.59	[55]
Phosphoric acid-modified orange peel cellulose	71.30	[55]
Raw lemon peels	20.83	[56]
NaOH-treated lemon peels	35.71	[56]
6-(2′-aminomethylpyridine)-6-deoxycellulose	5.48	[57]

as the precursor, an efficient biosorbent of high carboxyl content was synthesized. The *'Manna_COOH'* was subsequently applied as a novel biosorbent for cobalt ion uptake. The characteristic surface chemistry, morphology and crystallinity of the synthesized *'Manna_COOH'* is typical of a good and quality biosorbent. The effect of the process variable suggested the pH dependence of the adsorption system. Similarly, the equilibrium and kinetic studies returned the Freundlich and pseudo-second-order model as the respective models of best fit. The study demonstrates the efficacy of the *'Manna_COOH'* during the cobalt ion binding which is credited to the presence of abundance oxygen-based surface functional groups.

REFERENCES

1. R. Chen, Y. Zhang, L. Shen, X. Wang, J. Chen, A. Ma and W. Jiang, *Chem. Eng. J.*, **268**, 348 (2015).
2. S. Zhuang, K. Zhu and J. Wang, *J. Clean. Prod.*, **285**, 124911 (2020).
3. M. Abbas, S. Kaddour and M. Trari, *J. Ind. Eng. Chem.*, **20**(3), 745 (2014).
4. A. R. Lucaci, D. Bulgariu, I. Ahmad, G. Lisă, A. M. Mocanu and L. Bulgariu, *Water*, **11**(8), 1565 (2019).
5. M. He, Y. Zhu, Y. Yang, B. Han and Y. Zhang, *Appl. Clay Sci.*, **54**(3-4), 292 (2011).
6. D. Joksimovic, I. Tomic, A. R. Stankovic, M. Jovic and S. Stankovic, *Food Chem.*, **127**(2), 632 (2011)
7. N. B. Haq, K. Rubina and A. H. Muhammad, *Iran. J. Chem. Chem. Eng.*, **30**(4), 81 (2011).
8. C. O. Aniagor and M. C. Menkiti, *Sigma*, **38**(3), 1073 (2020).
9. A. Hashem, *Polym. Plast. Technol. Eng.*, **45**(1), 35 (2006).
10. A. Hashem, A. Abdel-Lateff, S. Farag and D. Hussein, *Adsorp. Sci. Technol.*, **26**(9), 661 (2008).
11. A. Hashem, E. Abdel-Halim, K. F. El-Tahlawy and A. Hebeish, *Adsorp. Sci. Technol.*, **23**(5), 367 (2005).
12. A. Hashem, A. Al-Anwar, N. M. Nagy, D. M. Hussein and S. Eisa, *Green Process. Synth.*, **5**(2), 213 (2016).
13. Z. Hubicki and D. Kołodyńska, *Ion exchange technologies*, Intech-Open, UK (2012).
14. Z. Wang, Y. Feng, X. Hao, W. Huang and X. Feng, *J. Mater. Chem.*, **2**(26), 10263 (2014).
15. N. Abdullah, N. Yusof, W. Lau, J. Jaafar and A. Ismail, *J. Ind. Eng. Chem.*, **76**, 17 (2019).
16. X. Fang, J. Li, X. Li, S. Pan, X. Zhang, X. Sun, J. Shen, W. Han and L. Wang, *Chem. Eng. J.*, **314**, 38 (2017).
17. C. Blöcher, J. Dorda, V. Mavrov, H. Chmiel, N. Lazaridis and K. Matis, *Water Res.*, **37**(16), 4018 (2003).
18. M. T. Yagub, T. K. Sen, S. Afroze and H. M. Ang, *Adv. Colloid Interface Sci.*, **209**, 172 (2014).
19. C. O. Aniagor and M. Menkiti, *Appl. Water Sci.*, **9**(4), 77 (2019).
20. C. O. Aniagor and M. Menkiti, *J. Environ. Chem. Eng.*, **6**(2), 2105 (2018).
21. M. C. Menkiti and C. O. Aniagor, *Arab. J. Sci. Eng.*, **43**(5), 2375 (2018).
22. S. Hua and A. Wang, *Polym. Adv. Technol.*, **19**(8), 1009 (2008).
23. A. Hashem, C. Aniagor, G. Taha and M. Fikry, *Current Res. Green Sustain. Chem.*, **4**, 100056 (2021).
24. S. Ayuba, A. A. Mohammadib, M. Yousefic and F. Changanic, *Desalination Water Treat.*, **142**, 293 (2019).
25. J. Wang and C. Chen, *Bioresour. Technol.*, **160**, 129 (2014).
26. R. Wang, R. Liang, T. Dai, J. Chen, X. Shuai and C. Liu, *Trends Food Sci. Technol.*, **91**, 319 (2019).
27. X. Liu, X. Xu, X. Dong and J. Park, *Pol. J. Environ. Stud.*, **29**(1), 749 (2020).
28. V. Thakur, E. Sharma, A. Guleria, S. Sangar and K. Singh, *Mater. Today: Proceedings*, **32**, 608 (2020).
29. E. Abdel-Halim and S. S. Al-Deyab, *React. Funct. Polym.*, **75**, 1 (2014).
30. K. Junlapong, P. Maijan, C. Chaibundit and S. Chantarak, *Int. J. Biol. Macromol.*, **158**, 258 (2020).
31. F. Balaska, M. Bencheikh-Lehocine, A.-H. Meniai, M. Chikhi and A. Bouledjouidja, *Energy Procedia*, **18**, 622 (2012).
32. A. Hashem, S. Badawy, S. Farag, L. Mohamed, A. Fletcher and G. Taha, *J. Environ. Chem. Eng.*, **8**(4), 103966 (2020).
33. A. Ebrahimi, M. Ehteshami and B. Dahrazma,. *Process Saf. Environ.*, **98**, 374 (2015).
34. M. Khalil, A. Hashem and A. Hebeish, *Starch-Stärke*, **42**(2), 60 (1990).
35. W. Gan, L. Gao, X. Zhan and J. Li, *RSC Adv.*, **6**(44), 37600 (2016).
36. M. L. Dianu, A. Kriza, N. Stanica and A. M. Musuc, *J. Serb. Chem. Soc.*, **75**(11), 1515 (2010).
37. B. Wang, M. Sain and K. Oksman, *Appl. Compos. Mater.*, **14**(2), 89 (2007).
38. A. Hashem, C. O. Aniagor, M. Nasr and A. Abou-Okeil, *Int. J. Biol. Macromol.*, **176**, 201 (2021).

39. C. O. Aniagor, M. Elshkankery, A. Fletcher, O. M. Morsy, E. Abdel-Halim and A. Hashem, *Water Conserv. Sci. Eng.*, **6**, 95 (2021).
40. C. A. Igwegbe, S. N. Oba, C. O. Aniagor, A. G. Adeniyi and J. O. Ighalo, *J. Ind. Eng. Chem.*, **93**, 57 (2020).
41. S. N. Oba, J. O. Ighalo, C. O. Aniagor and C. A. Igwegbe, *Sci. Total Environ.*, **780**, 146608 (2021).
42. C. O. Aniagor, C. A. Igwegbe, J. O. Ighalo and S. N. Oba, *J. Mol. Liq.*, **334**, 116124 (2021).
43. Y. Kuang, X. Zhang and S. Zhou, *Water*, **12**(2), 587 (2020).
44. E. Asuquo, A. Martin, P. Nzerem, F. Siperstein and X. Fan, *J. Environ. Chem. Eng.*, **5**(1), 679 (2017).
45. F. Gorzin and M. Bahri Rasht Abadi, *Adsorp. Sci. Technol.*, **36**(1-2), 49 (2018).
46. N. Thi Minh Tam, Y. Liu, H. Bashir, Z. Yin, Y. He and X. Zhou, *Int. J. Environ. Res. Public Health*, **17**(1), 291 (2020).
47. J. Elliott and C. Ward, *Langmuir*, **13**(5), 951 (1997).
48. C. O. Aniagor, E. Abdel-Halim and A. Hashem, *J. Environ. Chem. Eng.*, **9**(4), 105703 (2021).
49. I. Langmuir, *J. Am. Chem. Soc.*, **38**(11), 2221 (1916).
50. A. W. Adamson and A. P. Gast, *Physical chemistry of surfaces*, John Wiley & Sons, Inc., New York (1967)
51. J. Wang and X. Guo, *J. Hazard. Matet.*, **390**, 122156 (2020).
52. X. Guo and J. Wang, *J. Mol. Liq.*, **288**, 111100 (2019).
53. A. Kadam, R. G. Saratale, S. Shinde, J. Yang, K. Hwang, B. Mistry, G. D. Saratale, S. Lone, D. Y. Kim and J. S. Sung, *Bioresour. Technol.*, **273**, 386 (2019).
54. A. Hashem, C. Aniagor, D. Hussein and S. Farag, *Cellulose*, **28**, 3599 (2021).
55. X. Li, Y. Tang, X. Cao, D. Lu, F. Luo and W. Shao, *Colloids Surf. A Physicochem. Eng.*, **317**(1-3), 512 (2008).
56. S. Singh and S. Shukla, *Int. J. Environ. Sci. Technol.*, **13**(1), 165 (2016).
57. E. C. Silva Filho, L. S. Santos Júnior, M. M. F. Silva, M. G. Fonseca, S. A. A. Santana and C. Airoldi, *Mat. Res.*, **16**(1), 79 (2013).